C. R. Geoscience 346 (2014) 190–199

Contents lists available at ScienceDirect

Comptes Rendus Geoscience

www.sciencedirect.com

Petrology, Geochemistry

Silicate melt inclusions in the Qiushuwan granitoids, northern Qinling belt, China: Implications for the formation of a porphyry Cu–Mo deposit as a reduced magmatic system

Lili Wang *, Dehui Zhang, Lu Tian

School of Earth Sciences and Resources, China University of Geosciences (Beijing), Beijing 100083, China

ARTICLE INFO

Article history:
Received 8 April 2014
Accepted after revision 16 May 2014
Available online 2 July 2014

Keywords:
Melt inclusion
Volatiles
Qiushuwan granitoids
Northern Qinling belt

ABSTRACT

Melt inclusions (MIs) in quartz from granitoids in the northern Qinling belt were studied using microthermometry and laser Raman spectroscopy. The total homogenization of melt inclusions occurs in a mean range between 1050 and 1100 °C. Laser Raman experiments reveal H_2O, C_2H_6, C_4H_6 and CH_4 as the dominant volatile compounds. Our results provide insights into the temperatures of magma crystallization and the dominantly reducing environment during the early magmatic stage. Based on ore mineralogy, and on the volatile species content in the MIs, we evidence firstly that the Qiushuwan porphyry Cu–Mo deposit in the Qinling–Dabie–Sulu orogenic belt was derived from a reduced magmatic system, emplaced at relatively deep domains more than 10 km deep, and secondly, that the magmas that are responsible for the generation of Qiushuwan were either derived from an inherently reduced source, or reduced during ascent and emplacement. The mechanism might have involved the assimilation of sedimentary material with minimal crustal interaction. The parental magmas likely underwent reduction essentially by loss of all of their SO_2 by degassing, as evidenced by the low S content in melt inclusions. These reduced materials provided adequate sulfur source for the formation of the porphyry Cu–Mo deposits with obvious zonation, which plays a key role in the mineralization; finally, we conclude that the reduced environment and the relatively deep domain of magma emplacement probably limited the extent of mineralization, generating only a relatively small Cu–Mo deposit in Qiushuwan, located within the northern Qinling accretionary belt.

1. Introduction

Many of the important Cu, Mo, and Au deposits around the world are associated with porphyry systems (Patrick and Marco, 2010; Richards, 2003). Recent studies (e.g., Smith et al., 2012; Sun et al., 2013) show that porphyry deposits are formed in either oxidized or reduced environments, as can be seen on the basis of the mineralogy of the host pluton, ores and associated alteration assemblages, and the nature of hydrothermal alteration. The classic model of Burnham and Ohmoto (1980) for ore mineralization involves fluids that are relatively oxidized, with higher temperature and higher f_{O_2} value varying between the hematite–magnetite (HM) and nickel–nickel oxide (NNO) oxygen buffers, and also hosts a large number of primary magnetite, hematite, and sulfates associated with oxidized Type-I granitoids (Smith et al., 2012; Sun et al., 2013). Experiments (e.g., Candela and Bouton, 1990) also showed that the high oxygen fugacity of magmas can improve the differentiation index of Mo residual fluid (Mo in fluid over Mo in silicate melt). Similar phenomena have been observed for porphyry

* Corresponding author.
E-mail address: lilywang.gsf@cugb.edu.cn (L. Wang).

http://dx.doi.org/10.1016/j.crte.2014.05.003
1631-0713/

copper deposits in eastern Tibet (Liang et al., 2006), and it has been widely accepted fact that porphyry Cu–Mo–Au deposits are usually related to fluids derived from highly oxidized magmas (e.g., Han et al., 2013; Li et al., 2012, 2014). Therefore, many workers (e.g., Han et al., 2013; Li et al., 2012) consider that the progressive increase in zircon Ce/Ce^{*} or oxygen fugacity of the magmas resulted in the progressive extraction of Mo, leading to the accumulation of this metal in porphyry and eventually forming giant Mo deposits. In marked contrast to the models on highly oxidized fluid systems, several other typical porphyry Cu–Mo–Au deposits show evidence of having formed from relatively reduced ore fluids with lower f_{O_2} less than or equal to the QFM buffer (quartz–fayalite–magnetite), and lack of primary hematite and sulfate minerals, but with abundant reduced mineral assemblages, such as chalcopyrite, molybdenite, pyrite, sphalerite, galena, and hypogene pyrrhotite (e.g., Gao et al., 2014; Rowins, 2000; Smith et al., 2012); in addition to H_2O, the ore fluids in these deposits contain significant amounts of CO_2 and CH_4.

The East Qinling–Dabie orogenic belt hosts the largest Mo ore deposits in the world, with measured reserves of 802.4 Mt of Mo metal (Mao et al., 2011). The majority of the Mo deposits in this orogenic belt are associated with granite porphyries (Chen et al., 2014; Mao et al., 2008, 2011; Zhu et al., 2010). However, the redox states of these granitoids and their significance to metallogenesis have not been fully investigated. The redox states of melts and fluids could influence the behavior of the metallogenic components, such as Mo, Cu and Au, etc., during magma evolution (Candela, 1997). Silicate melt inclusions (MIs) are small (~1 to 300 μm) droplets of silicate melt that are trapped within phenocryst minerals in magmatic rocks. They are glassy or crystalline, and are found within both extrusive and intrusive rocks. Since many MIs form at high pressures and are enclosed within relatively robust phenocryst hosts, they may also preserve the traces of volatile elements that normally escape from magmas during degassing, even though the bulk magma decompresses to surface pressure during eruption. The careful analysis of quenched MIs can provide important information on the history of magma evolution and the role of volatile compounds (Anderson et al., 2000; Chesner and Luhr, 2010; Lowenstern, 1995). Quartz is one of the best minerals for inclusion studies because of its transparent and simple composition, which allows minimal chemical exchange with the included melt (Chesner and Luhr, 2010). In this study, we investigate melt inclusions in quartz from ore-bearing granitoids in the northern Qinling belt using microthermometry and laser Raman spectroscopy. Our results provide insights into the temperatures of magma crystallization and the role of volatiles.

2. Regional geology

The Qinling–Tongbai–Hong'an–Dabie–Sulu orogenic belt was developed through the Paleozoic convergence between the South China and North China cratons involving a series of tectonic processes including subduction–accretion–collision (Wu and Zheng, 2013, and references therein). Arc–continent collision and continent–continent collision dominated during the Early Mesozoic in the Dabie–Sulu orogens. The Qinling Orogen is considered to have evolved from the closure of the northernmost Paleo-Tethys Ocean and finally through the Mesozoic collision between the North China Craton and the blocks separated from Gondwana, such as the Yangtze Craton (Fig. 1A and B; Chen et al., 2009; Deng et al., 2013; Dong et al., 2011; Li et al., 2012; Wang and Shu, 2012; Wu and Zheng, 2013; Zhang et al., 2012). The Qinling Orogen is divided into four major tectonic units as follows: the Huaxiong block, which is the reactivated southern margin of the North China Craton; the northern Qinling accretionary belt; the southern Qinling orogenic belt; the foreland fold-thrust belt (e.g., the Songpan fold-thrust belt) along the northern margin of the Yangtze Craton. These four tectonic units are separated by the San-Bao, Luanchuan, Shang-Dan, Mian-Lue, and Longmenshan faults (Fig. 1B). In a recent synthesis, Deng et al. (2013) identified that among the 25 Mo deposits in the Eastern Qinling Molybdenum Belt (EQMB), 22 occur in the Huaxiong Block, with the remaining three small deposits being located within the northern Qinling accretionary belt (Fig. 1C).

The northern Qinling accretionary belt is bound to the south by the Shang-Dan fault, and to the north by the Luanchuan fault, which is considered as the southern boundary fault of the North China Craton (Chen et al., 2004). The main lithostratigraphic units of the northern Qinling belt include the Qinling Group, the Erlangping Group, and the Kuanping Group from south to north (Deng et al., 2013; Zhang et al., 2011). The Qinling Group, distributed between Zhu-Xia fault and Shang-Dan fault, is composed of gneisses, amphibolites, and marbles, and was mostly metamorphosed to amphibolite facies, and partly to granulite facies with ages ranging from the Neoproterozoic to the Early Paleozoic (Deng et al., 2013; Zhang et al., 2011). The protoliths of these rocks are commonly interpreted as being dominated by volcanic and sedimentary rocks formed in a Neoproterozoic–Ordovician volcanic arc (Hu et al., 1988; Zhang et al., 2001, 2009). The Erlangping Group, located to the north of Qinling Group and to the south of Kuanping Group, and separated by faults, is composed of an ophiolite unit, of metamorphosed clastic sedimentary rocks and carbonates, where the ophiolite unit includes ultramafic rocks, mafic lavas, and a small amount of radiolarian cherts (Dong et al., 2010; Zhang et al., 2011). The Kuanping Group to the north of the Erlangping Group is composed of highly deformed greenschist facies rocks, the protoliths of which comprise mainly basic volcanic rocks, clastic rocks and carbonates with Meso-Neoproterozoic ages (Zhang et al., 2001). All these three tectono-stratigraphic units in the northern Qinling area were accreted to the North China Craton before Devonian, and intruded by Late Paleozoic to Mesozoic granitoids (Chen et al., 2004; Hu et al., 1988).

3. Deposit geology

The Qiushuwan Cu–Mo porphyry–skarn deposit was the first Mo deposit to be discovered in the northern Qinling accretionary belt in the 1980s, and the deposit was formed in the Late Jurassic (ca. 148 Ma), associated with the Yanshanian orogeny, as estimated from Re–Os dating

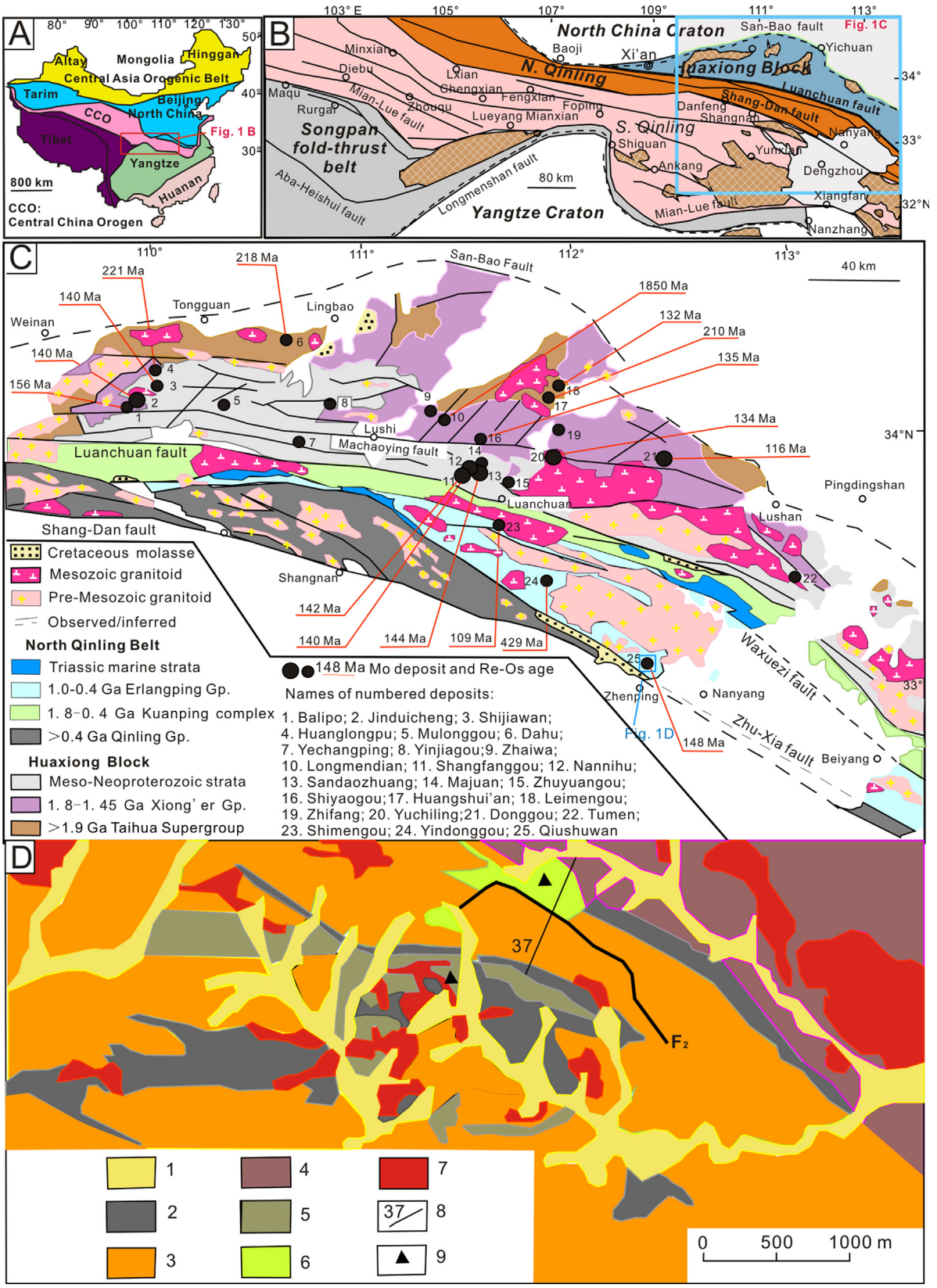

Fig. 1. (Color online). Schematic map showing the geology and tectonic setting of the Qiushuwan Mo–Cu deposit, Henan province. (A) Tectonic units of China and position of the Qinling Orogen; (B) tectonic subdivision of Qinling Orogen, showing the location of East Qinling Mo Belt; (C) distribution of Mo

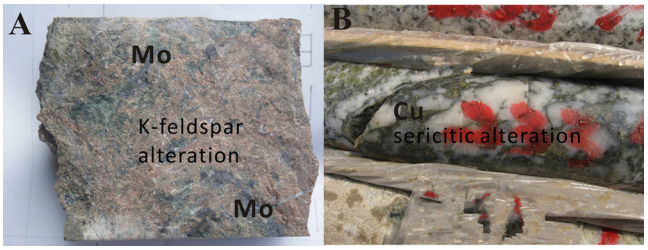

Fig. 2. (Color online). (A) Mo mineralization in Qiushuwan deposit associated with K-feldspar alteration; (B) Cu mineralization related to sericitic alteration.

of molybdenite mineralization (Guo, 2006; Guo et al., 2006; Mao et al., 2011). The deposit is hosted by the Early Proterozoic Qinling Group and the Yanlinggou and Guozhuang formations in the eastern margin of the northern Qinling accretionary belt, and to the north of Zhu-Xia fault (Fig. 1C and D) (Guo, 2006; Guo et al., 2006). The major metal in the Qiushuwan deposit is Cu, which distinguishes this deposit from the other porphyry systems in the East Qinling–Dabie belt (Mao et al., 2011), which are Mo-rich porphyry deposits.

The Qiushuwan porphyry Cu–Mo deposit (Fig. 1C) has a proven reserve of 500 kt of Cu with local ore grade averaging at 0.8% and 100 kt of Mo averaging at 0.12% (Guo et al., 2006; Mao et al., 2008). It is crosscut by several NE-trending faults like in the other Mo deposits along the southern margin of the North China Craton. A number of Mesozoic biotite granodiorite stocks hosting the mineralization were emplaced along the intersection of these NE-trending faults and WNW-trending thrust faults leading to the typically irregular shapes of the stocks, with area extents of about 0.06 km^2 (nearly 300 m long from east to west, 200 m wide from south to north) (Guo et al., 2006), and intruded into Early Proterozoic biotite gneissic rocks, biotite quartz schist, plagioclase amphibolites and marble (Mao et al., 2011, and their Fig. 17). Previous studies show that the Cu–Mo mineralization of the deposit is of two distinct types with obvious zonation regionally:

- a Mo-dominant skarn type along the southern contact of the Qiushuwan granodiorite stock;
- a Cu-dominant style within a 1000 m-long NE-striking breccia pipe (Guo, 2006; Mao et al., 2008, 2011; Qin et al., 2012).

The Cu–Mo mineralization is associated with siliceous, K-feldspar, sericitic, calc-silicate (skarn) and propylitic alteration. The Mo mineralization is associated with the K-feldspar alteration (Fig. 2A), whereas the Cu mineralization is related to sericitic and skarns (Fig. 2B). The major ore minerals include chalcopyrite, molybdenite, pyrite, sphalerite, galena and pyrrhotite, and the main gangue minerals are quartz, epidote, calcite, and diopside (Guo et al., 2006; Mao et al., 2011).

Based on the mineral assemblages, ore fabrics, wall-rock alteration and cross cutting veins, the mineralization stages in the Qiushuwan deposit can be divided into early (I), middle (II) and late (III), in which stage I is subdivided into four substages: prograde skarn-K-feldspar-quartz (I_1), crypto-explosive breccias (I_2), retrograde hydrous skarn (I_3), and magnetite stages(I_4); stage II includes porphyry Cu(Mo) mineral stage, and quartz–sulfide stage; stage III comprises calcite, barite and quartz (Qin et al., 2012). Qin et al. (2012) measured the homogenization temperatures of fluid inclusions from these stages, which are 222–406 °C for stage I, 152–315 °C for stage II and 119–189 °C for stage III; the salinities of these three stages are 4.2%–36.5%, 3.3%–34.8%, and 4.2%–11.9%, respectively. Qin et al. (2012) suggested that the early stage fluids of Qiushuwan deposit were high temperature, high-salinity, CO_2-bearing H_2O–NaCl–CO_2 magmatic fluids, and experienced boiling and phase separation during stage I, and thus deduced that fluid boiling, typically with CO_2 escape, temperature drop, addition of meteoric water, and decrease in salinity, results in the precipitation of metal sulfides of this deposit; in stages II and III, the ore-forming system became open, and meteoric water mixed with the hydrothermal solutions, evolving into the late low-salinity, low-temperature, poor-CO_2 fluid system.

Several studies show that the Qiushuwan granites related to Cu–Mo mineralization are geochemically similar to other highly fractionated Jurassic Type–I granites within the Qinling orogen (Fu, 2003; Guo, 2006; Mao et al., 2008, 2011; Qin et al., 2011). High Ba–Sr features from this granite were reported (Qin et al., 2011; Zhang et al., 2002), combined stable H and O isotope compositions with characteristics of mantle source, suggesting that the metallogenic components were derived from the lower crust and partly from the upper mantle (Guo, 2006; Guo et al., 2006; Qin et al., 2011, 2012; Zhang et al., 2002, 2011).

4. Analytical methods

4.1. Melt inclusion sampling and petrography

Samples used for melt inclusion study were collected from the granite porphyry and quartz porphyry in the Qiushuwan deposit with emphasis on the vein types and alterations. Nine thin sections were used for petrographic melt inclusion studies and then analyzed by microthermometry and laser Raman spectroscopy. Quartz phenocrysts

deposits in the Eastern Qinling Molybdenum Belt, showing the location of the Qiushuwan deposit; (D) geology of the Qiushuwan Mo–Cu deposit (modified after Guo et al., 2006; Deng et al., 2013; Li et al., 2012). [Legend for D: 1: Quaternary loess; 2: Lower Proterozoic amphibolites schist, Qinling Group, Shicaogou Formation; 3: Lower Proterozoic marble, Qinling Group, Guangzhuang Formation; 4: Lower Proterozoic granitic gneiss, Qinling Group, Yanlinggou Formation; 5: skarn; 6: breccias with Cu; 7: Yanshanian granite and granite porphyry; 8: exploration line and number; 9: sample location].

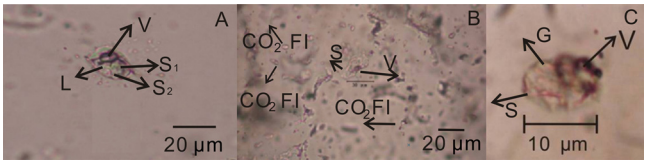

Fig. 3. (Color online). Representative melt inclusion types in the Qiushuwan porphyry Cu–Mo deposit. (A) Crystallized melt inclusion composed of two types of solids (S_1 and S_2), vapor (V) and liquid (L); (B) microcrystallized melt inclusion with vapor (V) coexists with several fluid inclusions containing vapor CO_2; (C) crystallized melt inclusion contains glass with one or more shrinkage bubbles(V).

with melt inclusions were used for this study, since they tend to survive the emplacement of the granitic intrusions and sample preparation without fracturing, and their homogeneous and constant composition makes data acquisition and reduction fairly simple (Lowenstern, 1995).

Fluid inclusions commonly occur in the quartz phenocrysts of the Qiushuwan porphyry Cu–Mo deposit and most of them contain CO_2 (Fig. 3B). Primary melt inclusions (MI) with unusually large vapor/melt ratios were avoided, as these inclusions might have lost volatile compounds during fracturing events (Lowenstern, 1995). The volumetric vapor/glass ratios in 18 MIs of the Qiushuwan porphyry Cu–Mo deposit show linear trend (Fig. 4), suggesting that they were trapped in a homogeneous state (Frezzotti, 2001).

MIs are relatively rare in the quartz phenocrysts of Qiushuwan deposit, and typically show a scattered or isolated distribution. They possess elliptical cavities 10–25 μm in diameter, and contain glass with one or more shrinkage bubbles (Fig. 3A and B). The MIs commonly contain several daughter crystals with one or more shrinkage bubbles, described herein as crystal-rich inclusions (Fig. 3A and C). These crystallized MIs were studied further for homogenization experiments and estimation of the water content with visually identical phase ratios and similar shapes (Goldstein and Reynolds, 1994).

4.2. Homogenization experiments

A high temperature heating stage was used to estimate entrapment temperatures of the MI by observing the temperature of homogenization of the shrinkage bubbles into the silicate melt (Touret and Huizenga, 2012). Ideally, homogenization indicates the minimum possible temperature of crystallization of the host phenocryst (Lowenstern, 1995). Most heating experiments in this study were performed on individual phenocrysts within doubly polished wafers with a thickness of ~1 mm, using a Linkam TS1500 heating stage with a Leitz optical microscope fitted with a CCD camera at the Institute of Geology and Geophysics, Chinese Academy of Sciences, China. The detailed procedures follow those of Thomas et al. (2000). Inclusions were remelted at temperatures of 700, 750, 800, 850, 900, 950, 1000, 1050, and 1100 °C using conventional hydrothermal rapid quench techniques. The total run duration was between 5 and 13 h; the higher the temperature, the longer the run duration to avoid the apparent homogenization temperature due to insufficient diffusion rates for water and other volatiles in MI allowing the bubble to dissolve into the melt within the time frame

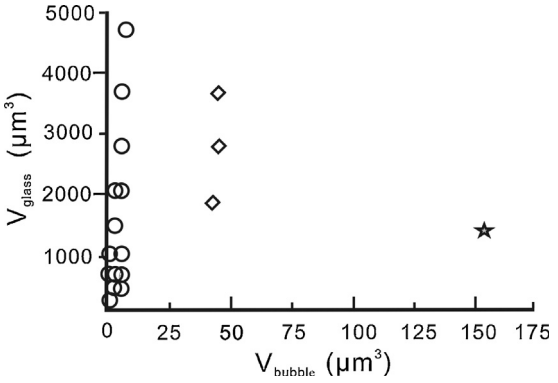

Fig. 4. Plot of V_{bubble} vs. V_{glass} in different MIs of the Quiushuwan porphyry Cu–Mo deposit. Circles and diamonds correspond to volumetric vapor/glass ratios in single inclusions, which trapped a homogeneous magma. The star indicates the volumetric vapor/glass ratio in the single inclusion that trapped differently from the above magma, probably in immiscible phases. Please note that the volumetric vapor/glass ratios in these MIs were calculated respectively according to the approximate radius of the bubble and the glasses, assuming that the melt inclusions and the bubbles inside are standard spheres. Redrawn after Tian (2009).

of the experiment (Lowenstern, 1995). For inclusions that homogenize at high temperatures, the initial run up to 700 °C was for 5 h. Subsequently, the run duration for every 50 °C heating step above 700 °C was 1 h. Thus, for those inclusions which homogenize at the highest temperature (1100 °C), the total run duration was 13 h. The remelted inclusions located at the polished surface of the quartz host were used for Raman spectroscopic analysis.

4.3. Laser Raman microspectroscopy

Laser Raman microspectroscopy has been effectively used for quantitatively determining water concentrations in the remelted silicate glasses. The technique is non-destructive, requires minimal sample preparation, and can be used to analyze both exposed and unexposed inclusions as small as 3 μm in diameter (Chabiron et al., 1999, 2004; Thomas et al., 2000). The technique and analytical details were described in detail by Chabiron et al. (2004), Muro et al. (2006), Severs et al. (2007), Thomas and Davidson (2007), Thomas et al. (2000), Zajacz et al. (2005), and have been applied to analyze concentrations from 0 to 20 wt.% within an accuracy of ± 0.2 wt.% (Thomas et al., 2000). Although the water content was not analyzed in this study due to experimental limitations, the data for H_2O concentration available in previous studies from this pluton (e.g., Tian, 2009) are used for interpretations in this study.

The homogenized melt inclusions of the Qiushuwan porphyry Cu–Mo deposit were used in this experiment after quenching. The gas analysis in melt inclusions was obtained using a RM-2000 Laser Raman microspectrometer at the State Key Laboratory of Lithospheric Evolution, Institute of Geology and Geophysics, Chinese Academy of Sciences, China. A grating of 600 was used and allowed us to record spectra ranging from 100 to 4000 cm^{-1}, covering, in one experiment, the area of the silicate framework at low wave numbers and the area of the water-stretching bands at high wave numbers. A CCD detector collected glass spectra with sample excitation produced by an argon laser beam (514 nm) at a power of 300 mW and with an acquisition time of 10 s. The laser beam is about 1 μm in diameter, and spectral resolution is 2 cm^{-1}.

5. Results

5.1. Microthermometric results

We analyzed the homogenization temperature of 28 melt inclusions in quartz phenocrysts from Qiushuwan granitoids to constrain the magmatic temperatures. Fig. 5 shows the evolution of a crystallized melt inclusion as it is heated from room temperature up to 1100 °C. During heating, the daughter crystals melt, the bubbles shrink, and in many cases disappear, resulting in a homogeneous melt at about 1100 °C; and the light color of melt inclusions overall tend to become dark in the initial heating stage, and gradually return to transparent near the homogenization temperature. Although not always possible, repeated cycling of temperature between 900 and 1000 °C can produce nucleation of hypersaline fluid bubbles (not shown in the figure) before reaching the final homogenization temperature. Some of the melt inclusions after remelting failed to quench homogenously and exsolved a liquid and a vapor phase even during rapid quenching, and in most cases, complete rehomogenization, that is, L + glass + crystals → melt, could not be observed at the heating stage because the inclusions decrepitated prior to attaining the necessary rehomogenization temperature. Thus, only nine melt inclusions in this study reached the final homogenization temperature, with an average temperature of 1050–1100 °C, suggesting that the inclusions were trapped from a homogenous melt at around 1100 °C. The initial melting of daughter crystals occurred at around 800 °C, and bubbles in melt inclusions started to shrink at 750–800 °C. Some of the vapor bubbles were reproduced at 900–1000 °C, and then gradually shrunk and disappeared while reaching the homogenization temperatures.

Furthermore, we noticed that the melt inclusions with larger size have relatively higher homogenization temperatures, and longer run durations (> 20 h). The melt inclusions with larger initial vapor/glass bubble volume ratios tend to have higher homogenization temperatures, the difference in homogenization temperatures being up to 150–200 °C.

5.2. Laser Raman microspectroscopy

We analyzed the laser Raman microspectrosocpy of the above nine melt inclusions with homogenization temperatures in the quartz phenocrysts from Qiushuwan to obtain information on the volatile components of the magma. Fig. 6 shows the main results from laser Raman experiments, which show that H_2O, C_2H_6, C_4H_6 and CH_4 are mainly present in the melt inclusions (the ranges of the Raman peak shift for these phases are: 3200–3750 for H_2O, 2945–2975 for C_2H_6, 1633–1653 for C_4H_6, and 2905–2925 for CH_4), lack oxidized volatile components, such as SO_2, CO_2, Cl^- etc., indicating a dominantly reducing environment at the trapping stage.

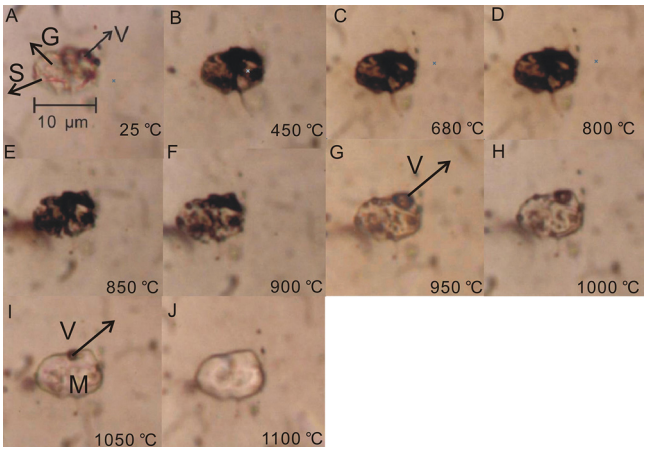

Fig. 5. (Color online). Behavior of fluid oversaturated silicate melt inclusions in quartz from the Qiushuwan granite during high temperature experiments. (A) At room temperature, the inclusion consists of partly devitrified glass (G), vapor (V), and salt (S). (B–E) While progressively heated, the inclusion remained microcrystalline up to 850 °C, and the color is getting dark (F) when melting began around the inclusion periphery at 900 °C. (G–I) The glass appears more transparent and the salt progressively melts in the silicate melt, and the single vapor bubble began to shrink in the inclusion; at 1050 °C the inclusion has not yet reached homogenization within 5 h duration of heating, and the crystals had mostly melted and all that remained was silicate melt (M), vapor bubbles (V). (J) At 1100 °C, the inclusion has reached Th, at which point the bubble had homogenized in the silicate melt, after having been heated during 8 h.

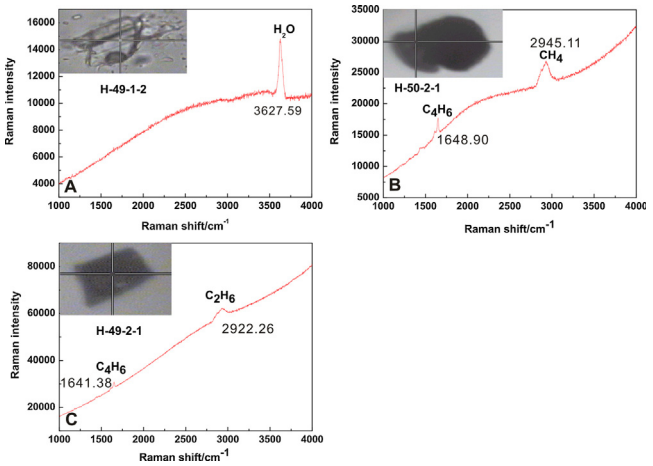

Fig. 6. (Color online). Laser Raman spectra of melt inclusions of the Qiushuwan deposit. A shows the presence of water vapor inside the melt inclusion; B shows that the melt inclusion includes gas bubbles of C_2H_6 and C_4H_6; C shows that C_4H_6 and CH_4 are present in the melt inclusion.

6. Discussion

6.1. Emplacement of the Qiushuwan granitoids

Magma contains many magmatic volatile components phases, such as, H_2O, CO_2, F, Cl, B, which play important roles in magma evolution and magmatite formation (Lowenstern, 1995; Wyllie and Ryabchikov, 2000). The magmatic volatile phase (MVP) is thought to be a critical agent in ore formation because of the high fluidity and buoyancy, and also the geochemical affinity (Candela, 1997). Plank et al. (2013) suggested that melt inclusion H_2O values reflect vapor saturation at the last storage depth in the crust prior to eruption. Although the water content was not analyzed in this study, the data for H_2O concentration in the melt inclusions of this region reported by Tian (2009) following the Raman spectroscopy technique on melt inclusions of Severs et al. (2007) show a range of 0.58 to 20.85 wt%, with an average of 7.27wt%, indicating a relatively high original H_2O concentration of the acidic silicate magma at this emplacement. According to the solution models of Newman and Lowenstern (2002) and Witham et al. (2012), a magma with 7 wt% H_2O will reach pure H_2O-vapor saturation at ca.400 MPa, or ca.15–16 km in the crust (assuming an upper crustal density of 2.6 g/cc). In this case, considering the arc tectonic setting of this region and also the porphyritic texture of the rocks, we could deduce that Qiushuwan granitoids magmas rise from the mantle with high temperatures (about 1100 °C from the homogenization experiment in this study), high H_2O values and other reduced volatiles, and become vapor-saturated at relatively deep domains, probably more than 10 km, in the crust prior to eruption.

6.2. Generation of reduced granitoid magmas and mineralization

During the Late Jurassic–Early Cretaceous, the East Qinling region was under post-collisional extensional setting (Ding et al., 2011; Liu and Zhang, 2008), and many porphyry and porphyry-skarn types of Cu and Mo ore deposits were formed during this second episode in the Qinling orogen (Mao et al., 2008), spatially and genetically associated with granitic porphyry intrusions (see Fig. 1). Several workers (e.g., Chen et al., 2014; Li et al., 2012) suggested that most of the ore-forming elements (Mo and Cu) in the Qinling Orogenic Belt were transported from the crystallizing magma into a hot, alkaline, and oxidized fluid in the initial stage, and precipitated with decreasing temperatures and pH, water–rock interaction, and fluid immiscibility during fluid ascent. However, the granite of the Qiushuwan deposit studied here shows evidence of having formed from a reduced magma, containing substantial C_2H_6, C_4H_6, and CH_4 in melt inclusions. Field observation shows that primary pyrrhotite is far more abundant than magnetite, and the ore system also shows reduced mineral assemblages, such as chalcopyrite, molybdenite, pyrite, sphalerite, galena, and pyrrhotite. Neither anhydrite nor hematite is present at Qiushuwan, and the abundant hypogene pyrrhotite suggests a relatively reducing ore fluid (Smith et al., 2012). These characteristics of the ore system are in conformity with the substantial C_2H_6, C_4H_6, and CH_4 contents found in the Qiushuwan granite, which are orders of magnitude higher than those typical of magmas associated with typical oxidized porphyry Cu deposits. The same studies were reported by Rowins (2000), who analyzed several reduced porphyry Cu–Mo–Au deposits, such as the Mile Hill (Western Australia), and San Anton (Mexico) deposits, and showed that the ore fluids of both deposits are compositionally complex. In addition to H_2O, the ore fluids in these deposits contain significant amounts of CO_2 and CH_4. The reduced fluids usually encountered in these cases typically lack primary hematite, magnetite, and sulfate minerals (i.e., anhydrite), but contain abundant hypogene pyrrhotite. The fluid inclusions are carbonic-rich with substantial CH_4, and are associated with ilmenite-bearing, reduced Type–I granitoids.

Some studies have proposed that the subduction of C- and S-rich sediments could lead to the production of

reduced arc magmas (Ague and Brimhall, 1988; Rowins, 2000; Takagi, 2004), which involves the significant input of reducing sedimentary material to a subduction zone to generate arc magmas. Qin et al. (2012) showed that some of the $\delta^{34}S$ values of pyrite from the Qiushuwan deposit have the characteristics of a sedimentary source of sulfur, suggesting that S-rich sediments might have been involved in magma genesis.

Rowins (2000) reported field evidence and low fluid-oxidation states that suggest that reduced porphyry Cu–Au deposits are intimately associated with reduced type-I granitoids, which could generated oxidized type-I partial melts, associated with oxidized porphyry Cu–Au deposits. Burham and Ohmoto (1980) and Rowins (2000) proposed that low f_{O_2} S-type granitoids could also exsolve reduced hydrothermal fluids, but these magmas are unlikely to be a factor in the genesis of reduced porphyry Cu–Au deposits. This is because S-type magmas associated with Sn–W deposits only contain about 10% of the S present in type-I granitoids and also contain much lower initial abundances of Cu and Au. They concluded that S-type granitoids are substantially reduced and contain neither sufficient S nor background metal components to produce economic porphyry Cu–Au mineralization. Thus, in our case, a possible alternate origin of the reduced materials is a parental type-I granite which might have acquired a low f_{O_2} value and have reduced materials during their ascent from the mantle through the crust, and subsequently have mixed with an S-type melt containing reduced materials. Such a mixing process has been described from orogenic belts elsewhere (e.g., Winter, 2001).

Ratschbacher et al. (2003) suggested that the Late Jurassic to Early Cretaceous granites of the Qinling Group in the East Qinling-Dabie have been associated with a continental magmatic arc on the north margin of Yangtze Craton. According to several studies (e.g., Carmichael, 1991; Lee et al., 2005; Smith et al., 2012), the magmas in arcs are typically more oxidized than in other tectonic settings. Several mechanisms have been invoked to generate oxidized magmas including fractional crystallization during ascent or emplacement, assimilation of oxidized country rock, or degassing of reduced volatile species (i.e., H_2, H_2S and CH_4) (Holloway, 2004; Lee et al., 2005). However, few mechanisms generate reduced magmas, especially in arc settings. Smith et al. (2012) proposed that one possibility for the generated reduced magmas is linked with the subduction of a mid-ocean ridge and the formation of a slab window, in which the slab window setting could form a pulse of lower f_{O_2} MORB-like mantle into the overriding mantle wedge, leading to a source region at a lower f_{O_2} than typical of arc magmas (Madsen et al., 2006). The geochemistry of the magmatic rocks of Qiushuwan suggests an arc signature (Fu, 2003; Guo, 2006; Mao et al., 2008, 2011; Qin et al., 2011; Zhang et al., 2002), but shows no geochemical evidence of derivation from a MORB or OIB-like mantle source (Guo et al., 2006; Mao et al., 2008, 2011).

The possibility that Qiushuwan Cu–Mo mineralization originates from reduced magma could be deduced and interpreted as such: it was formed by remelting of the lower crust caused by asthenospheric mantle upwelling, with the magma ascending along the intersection of existing NWW-trending regional faults and newly developed NNE-trending faults (Mao et al., 2005). The magma might have been an initially reduced type-I magma containing volatile compounds such as CH_4, or got reduced during ascent and emplacement with volatiles such as SO_2 through reaction with S-bearing sources under specific physicochemical conditions and crystal fractionation processes. Following magmatic fractionation during their ascent toward shallow levels of the crust, the generated S^{2-}could prevent the formation of sulfate minerals (e.g., anhydrite), but could easily combine with the metallogenic element, Mo, to cause molybdenite mineralization from magma in the fluid phase to the melt phase, whereas other metallic elements (e.g., Cu and Au) have a tendency to accumulate in the fluid phase of magma because of their strong chemical activities under reduced environment, and to accumulate and precipitate in favorable locations of the magma chambers and their immediate host rocks, but probably far away from the granite systems. Therefore, it is probably the reason why a distinct Cu–Mo mineralization formed in the studied area compared with other deposits in the Qinling Orogen, with Cu-rich compounds and the obvious zonation of Cu–Mo mineralization regionally.

7. Conclusions

Based on ore mineralogy, and volatile species in MIs, we identified that the Yanshanian Qiushuwan porphyry Cu–Mo deposit in the Qinling–Dabie orogenic belt is a reduced homogeneous magmatic system with high temperature (about 1100 °C), emplaced in relatively deep domains, probably more than 10 km deep. Magmas responsible for the generation of Qiushuwan were either derived from an inherently reduced source, or were reduced during ascent and emplacement. The mechanism might have involved the assimilation of sedimentary material with minimal crustal interaction. Parental magmas likely underwent reduction essentially by loss of all of its SO_2 by degassing, as evidenced by the low S level in MIs. These reduced materials provided an adequate sulfur source for the formation of the porphyry Cu–Mo deposits with obvious zonation, which plays a key role in the mineralization. In this regard, the reduced environment and the relatively deep domain of magma emplacement probably limited the extent of mineralization, generating only a relatively small Cu–Mo deposit in Qiushuwan.

Disclosure of interest

The authors declare that they have no conflicts of interest concerning this article.

Acknowledgement

We are thankful for the constructive review comments from Prof. Franco Pirajno and Prof. T. Tsunogae on an early version of the manuscript. We also thank Prof. M. Santosh for his valuable help with the revision of manuscript. The study is supported by the Natural Science Foundation of

China (Grant No. 41373048) and Ministry of Land and Resources Public Benefit Research Foundation of China (Grant No. 201411024).

References

Ague, J.J., Brimhall, G.H., 1988. Magmatic arc asymmetry and distribution of anomalous plutonic belts in batholiths of California: effects of assimilation, crustal thickness, and depth of crystallization. Geol. Soc. Am. Bull. 100, 912–927.

Anderson, A.T., Davis, A.M., Lu, F.Q., 2000. Evolution of Bishop Tuff Rhyolitic Magma Based on Melt and Magnetite Inclusions and Zoned Phenocrysts. J. Petrol. 41, 449–473.

Burnham, C.W., Ohmoto, H., 1980. Late-stage processes of felsic magmatism. Min. Geol. 8 (special issue), 1–12.

Candela, P.A., 1997. A review of shallow, ore-related granites: textures, volatiles, and ore metals. J. Petrol. 38, 1619–1633.

Candela, P.A., Bouton, S.L., 1990. The influence of oxygen fugacity on tungsten and molybdenum partitioning between silicate melts and ilmenite. Econ. Geol. 85, 633–640.

Carmichael, I.S.E., 1991. The redox states of basic and silicic magmas: a reflection of their source regions? Contrib. Mineral. Petrol. 106, 129–141.

Chabiron, A., Peiffert, C., Pironon, J., Cuney, M., 1999. Determination of water content in melt inclusions by Raman spectrometry. In: Ristedt, H., Luders, V., Thomas, R., Schmidt-Mumm, A. (Eds.), European Current Research on Fluid Inclusions. (AbstrProg., Terra Nostra- Schr. Alfred-Wegner-Stiftung 99/6), pp. 68–69.

Chabiron, A., Pironon, J., Massare, D., 2004. Characterization of water in synthetic rhyolitic glasses and natural melt inclusions by Raman spectroscopy. Contrib. Mineral. Petrol. 146, 485–492.

Chen, X.D., Ye, H.S., Wang, H., 2014. Genesis and evolution of the Leimengou porphyry Mo deposit in West Henan Province, East Qinling–Dabie belt, China: Constraints from hydrothermal alteration, fluid inclusions and stable isotope data. J. Asian Earth Sci. B 79, 710–722.

Chen, Y.J., Pirajno, F., Sui, Y.H., 2004. Isotope geochemistry of the Tieluping silver deposit, Henan, China: a case study of orogenic silver deposits and related tectonic setting. Miner. Deposita 39, 560–575.

Chen, Y.J., Pirajno, F., Li, N., Guo, D.S., Lai, Y., 2009. Isotope systematics and fluid inclusion studies of the Qiyugou breccia pipe-hosted gold deposit, Qinling Orogen, Henan province, China: implications for ore genesis. Ore Geol. Rev. 35, 245–261.

Chesner, C.A., Luhr, J.F., 2010. A melt inclusion study of the Toba Tuffs, Sumatra, Indonesia. J. Volcanol. Geoth. Res. 259–278.

Deng, X.H., Chen, Y.J., Santosh, M., Zhao, G.C., Yao, J.M., 2013. Metallogeny during continental outgrowth in the Columbia supercontinent: Isotopic characterization of the Zhaiwa Mo–Cu system in the North China Craton. Ore Geol. Rev. 51, 43–56.

Ding, L.X., Ma, C.Q., Li, J.W., Robinson, P.T., Deng, X.D., Zhang, C., Xu, W.C., 2011. Timing and genesis of the adakitic and shoshonitic intrusions in the Laoniushan complex, southern margin of the North China Craton: Implications for post-collisional magmatism associated with the Qinling Orogen. Lithos 126 (3–4), 212–232.

Dong, Y.P., Genser, J., Neubauer, F., Zhang, G.W., Liu, X.M., Yang, Z., Heberer, B., 2011. U–Pb and $^{40}Ar/^{39}Ar$ geochronological constraints on the exhumation history of the North Qinlingterrane, China. Gondwana Res. 19, 881–893.

Dong, Y.P., Zhang, G.W., Hauzenberger, C., Neubauer, F., Zhao, Y., Liu, X.M., 2010. Palaeozoic tectonics and evolutionary history of the Qinling orogen: Evidence from geochemistry and geochrofnology of ophiolite and related volcanic rocks. Lithos, http://dx.doi.org/10.1016/j.lithos.2010.11.011.

Frezzotti, M.-L., 2001. Silicate-melt inclusions in magmatic rocks: applications to petrology. Lithos 55, 299–573.

Fu, X., 2003. Genesis of Qiushuwan copper(molybdenum) deposit of Henan Province. Miner. Resour. Geol. 17 (3), 233–236 (in Chinese with English Abstract).

Gao, M.J., Qin, K.Z., Li, G.M., Jin, L.Y., Evans, N.J., Yang, X.R., 2014. Baogutu: An example of reduced porphyry Cu deposit in western Junggar. Ore Geol. Rev. 56, 159–180.

Goldstein, R.H., Reynolds, T.J., 1994. Systematics of fluid inclusions in diagenetic minerals, 31. Society for Sedimentary Geology Short Course, 199 p.

Guo, B.J., 2006. Study on the Mesozoic metallogenic associations and regularities of the east Qinling, China. China University of Geosciences (Beijing) (Ph.D. thesis).

Guo, B.J., Mao, J.W., Li, H.W., Qu, W.J., Qiu, J.J., Ye, H.S., Li, M.W., Zhu, X.L., 2006. Re–Os dating of the molybdenite from the Qiushuwan Cu–Mo deposit in the East Qinling and its geological significance. Acta Petrol. Sin. 22, 2141–2148 (in Chinese with English abstract).

Han, Y.G., Zhang, S.H., Pirajno, F., Zhou, X.W., Zhao, G.C., Qu, W.J., Liu, S.H., Zhang, J.M., Liang, H.B., Yang, K., 2013. U–Pb and Re–Os isotopic systematics and zircon Ce^{4+}/Ce^{3+} ratios in the Shiyaogou Mo deposit in eastern Qinling, central China: Insights into the oxidation state of granitoids and Mo (Au) mineralization. Ore Geol. Rev. 55, 29–47.

Holloway, J.R., 2004. Redox reactions in seafloor basalts: possible insights into silicic hydrothermal systems. Chem. Geol. 210, 225–230.

Hu, S.X., Lin, Q.L., Chen, Z.M., Li, S.M., 1988. Geology and Metallogeny of the Collision Belt between the South China and North China Plates. Nanjing University Press, Nanjing (558 p. [in Chinese]).

Lee, C.A., Leeman, W.P., Canil, D., Li, Z.A., 2005. Similar V/Sc systematics of MORB and arc basalts: implications for the oxygen fugacities of their mantle source regions. J. Petrol. 46, 2313–2336.

Li, H.Y., Ye, H.S., Wang, X.X., Yang, L., Wang, X.Y., 2014. Geology and ore fluid geochemistry of the Jinduicheng porphyry molybdenum deposit, East Qinling, China. J. Asian Earth Sci. 79, 641–654.

Li, N., Chen, Y.J., Pirajno, F., Gong, H.J., Mao, S.D., Ni, Z.Y., 2012. LA-ICP-MS zircon U–Pb dating, trace element and Hf isotope geochemistry of the Heyu granite batholith, eastern Qinling, central China: implications for Mesozoic tectono-magmatic evolution. Lithos 142–143 (34–47).

Liang, H.Y., Campbell, I.H., Allen, C., Sun, W.D., Liu, C.Q., Yu, H.X., Xie, Y.W., Zhang, Y.Q., 2006. Zircon Ce^{4+}/Ce^{3+} ratios and ages for Yulong ore-bearing porphyries in eastern Tibet. Miner. Deposita 41, 152–159.

Liu, S.F., Zhang, G.W., 2008. Evolution and geodynamics of basin/mountain systems in East Qinling-Dabieshan and its adjacent regions, China. Geol. Bull. China 27 (12), 1943–1960 (in Chinese with English Abstract).

Lowenstern, J.B., 1995. Applications of silicate melt inclusions to the study of magmatic volatiles. In: Thompson, J.F.H. (Ed.), Magmas, Fluids and Ore Deposits, Volume #23, Mineralogical Association of Canada Short Course, pp. 71–99.

Madsen, J., Thorkelson, J., Friedman, R., Marshall, D., 2006. Cenozoic to recent plate configurations in the Pacific Basin: ridge subduction and slab window magmatism in western North America. Geosphere 2, 11–34.

Mao, J.W., Xie, G.Q., Bierlein, F., Qu, W.J., Du, A.D., Ye, H.S., Pirajno, F., Li, H.M., Guo, B.J., Li, Y.F., Yang, Z.Q., 2008. Tectonic implications from Re-Os dating of Mesozoic molybdenum deposits in the East Qinling-Dabieorogenic belt. Geochim. Cosmochim. Acta 72, 4607–4626.

Mao, J.W., Pirajno, F., Xiang, J.F., Gao, J.J., Ye, H.S., Li, Y.F., Guo, B.J., 2011. Mesozoic molybdenum deposits in the East Qinling–Dabieorogenic belt: Characteristics and tectonic settings. Ore Geol. Rev. 43, 264–293.

Muro, A.D., Villemant, B., Montagnac, G., 2006. Quantification of water content and speciation in natural silicic glasses (phonolite, dacite, rhyolite) by confocal microRaman spectrometry.Geochim. Cosmochim. Acta 70, 2868–2884.

Newman, S., Lowenstern, J.B., 2002. VOLATILECALC: a silicate–melt–H_2O–CO_2 solution model written in Visual Basic for Excel. Comput. Geosci. 28, 597–604.

Patrick, B.R., Marco, T.E., 2010. The Bingham Canyon Porphyry Cu–Mo-Au deposits. I. Sequence of intrusion, vein formation, and sulfide deposition. Econ. Geol. 105, 43–68.

Plank, T., Kelley, K.A., Zimmerc, M.M., Haurid, E.H., Wallace, P.J., 2013. Why do mafic arc magmas contain ≈4 wt% water on average? Earth Planet. Sci. Lett. 364, 168–179.

Qin, Z., Dai, X.L., Deng, X.W., 2011. Two different granites in Qiushuwan and Yanlailing area, East Qinling orogenic belt and their tectonic significance. J. Mineral. Petrol. 31 (3), 48–54 (in Chinese with English Abstract).

Qin, Z., Dai, X.L., Deng, X.W., 2012. Fluid inclusions and stable isotopes of Qiushuwan copper-molybdenum deposit in East Qinling orogenic belt and their geological implications. Miner. Deposits 31 (2), 323–336 (in Chinese with English Abstract).

Ratschbacher, L., Hacker, B.R., Calvert, A., Webb, L.E., Grimmer, J.C., McWilliams, M.O., Ireland, T., Dong, S.W., Hu, J.M., 2003. Tectonics of the Qinling (Central China): tectonostratigraphy, geochronology, and deformation history. Tectonophysics 366, 1–53.

Richards, J.P., 2003. Tectono-Magmatic Precursors for Porphyry Cu-(Mo-Au) Deposit Formation. Econ. Geol. 98 (8), 1515–1533.

Rowins, S.M., 2000. Reduced porphyry copper–gold deposits: a new variation on an old theme. Geology 28, 491–494.

Severs, M.J., Azbej, T., Thomas, J.B., Mandeville, C.W., Bodnar, R.J., 2007. Experimental determination of H_2O loss from melt inclusions during laboratory heating: Evidence from Raman spectroscopy. Chem. Geol. 237, 358–371.

Smith, C.M., Canil, D., Rowins, S.M., Friedman, R., 2012. Reduced granitic magmas in an arc setting: the Catface porphyry Cu–Mo deposit of the Paleogene Cascade Arc. Lithos 154, 361–373.

Sun, W.D., Liang, H.Y., Ling, M.X., Zhan, M.Z., Ding, X., Zhang, H., Yang, X.Y., Li, Y.L., Ireland, T.R., Wei, Q.R., Fan, W.M., 2013. The link between reduced porphyry copper deposit and oxidized magmas. Geochim. Cosmochim. Acta 103, 263–275.

Takagi, T., 2004. Origin of magnetite- and ilmenite-series granitic rocks in the Japan Arc. Am. J. Sci. 304, 169–202.

Thomas, R., Davidson, P., 2007. Progress in the determination of water in glasses and melt inclusions with Raman spectroscopy: A short review. Acta Petrol. Sin. 23 (1), 15–20.

Thomas, R., Webster, J.D., Heinrich, W., 2000. Melt inclusion in pegmatite quartz: complete miscibility between silicate melts and hydrous fluids at low pressure. Contrib. Mineral. Petrol. 139, 394–401.

Tian, L., 2009. Tests of homogenization temperature and volatile content of melt inclusions (M.S. thesis). China University of Geosciences (Beijing), 40–55 (in Chinese with English Abstract).

Touret, J.L.R., Huizenga, J.M., 2012. Charnockite microstructures: from magmatic to metamorphic. Geosci. Front. 3 (6), 745–753.

Wang, D.Z., Shu, L.S., 2012. Late Mesozoic basin and range tectonics and related magmatism in Southeast China. Geosci. Front. 3 (2), 109–124.

Winter, J.D., 2001. An Introduction to igneous and metamorphic petrology. Upper Saddle, New Jersey343–361.

Witham, F., Blundy, J., Kohn, S., Lesne, P., Dixon, J., Churakov, S.V., Botcharnikov, R., 2012. SolEx: a model for mixed COHSCl-volatile solubilities and exsolved gas compositions in basalt. Comput. Geosci. 45, 87–97.

Wu, Y.B., Zheng, Y.F., 2013. Tectonic evolution of a composite collision orogen: An overview on the Qinling–Tongbai–Hong'an–Dabie–Sulu orogenic belt in central China. Gondwana Res. 23, 1402–1428.

Wyllie, P., Ryabchikov, I.D., 2000. Volatile components, magmas, and critical fluids in upwelling Mantle. J. Petrol. 41, 1195–1206.

Zhang, Z.W., Yang, H.Z., Zhu, B.Q., Deng, J., 2002. Endogenic metallogenic system and assemblage in the East Qinling, China. Geol. Bull. China 21, 567–572 (in Chinese with English abstract).

Zhang, J., Chen, Y.J., Qi, J.P., Ge, J., 2009. Comparison of the typical metallogenic systems in the North Slope of the Tongbai-East Qinling Mountains and its geologic implications. Acta Geol. Sin. 83, 396–410.

Zhang, J., Ma, C., She, Z., 2012. An Early Cretaceous garnet-bearing metaluminous A type granite intrusion in the East Qingling Orogen, central China: petrological, mineralogical and geochemical constraints. Geosci. Front. 3, 635–646.

Zhang, J.X., Yu, S.Y., Meng, F.C., 2011. Ployphase Early Paleozoic metamorphism in the northern Qinling orogenic belt. Acta Petrol. Sin. 27 (4), 1179–1190.

Zhang, G.W., Zhang, B.R., Yuan, X.C., Xiao, Q.H., 2001. Qinling orogenic and Continental Dynamics. Science Press, Beijing1–806 (in Chinese with English Abstract).

Zajacz, Z., Halter, W., Malfait, W.J., Bachmann, O., Bodnar, R.J., Hirschmann, M.M., Mandeville, C.W., Morizet, Y., Müntener, O., Ulmer, P., Webster, J.D., 2005. A composition-independent quantitative determination of the water content in silicate glasses and silicate melt inclusions by confocal Raman spectroscopy. Contrib. Mineral. Petrol. 150, 631–642.

Zhu, L.M., Zhang, G.W., Guo, B., Lee, B., Gong, H.J., Wang, F., 2010. Geochemistry of the Jinduicheng Mo-bearing porphyry and deposit, and its implications for the geodynamic setting in East Qinling, P.R China. Chem. Erde-Geochem. 70 (2), 159–174.